https://ntrs.nasa.gov/search.jsp?R=20160009114 2019-08-31T02:04:13+00:00Z

NASA/TM—2016-219124

Multiscale Modeling of Carbon/Phenolic Composite Thermal Protection Materials: Atomistic to Effective Properties

Steven M. Arnold, Pappu L. Murthy, and Brett A. Bednarcyk
Glenn Research Center, Cleveland, Ohio

John W. Lawson
Ames Research Center, Moffett Field, California

Joshua D. Monk
Analytical Mechanics, Inc., Moffett Field, California

Charles W. Bauschlicher, Jr.
Ames Research Center, Moffett Field, California

July 2016

NASA STI Program . . . in Profile

Since its founding, NASA has been dedicated to the advancement of aeronautics and space science. The NASA Scientific and Technical Information (STI) Program plays a key part in helping NASA maintain this important role.

The NASA STI Program operates under the auspices of the Agency Chief Information Officer. It collects, organizes, provides for archiving, and disseminates NASA's STI. The NASA STI Program provides access to the NASA Technical Report Server—Registered (NTRS Reg) and NASA Technical Report Server—Public (NTRS) thus providing one of the largest collections of aeronautical and space science STI in the world. Results are published in both non-NASA channels and by NASA in the NASA STI Report Series, which includes the following report types:

- TECHNICAL PUBLICATION. Reports of completed research or a major significant phase of research that present the results of NASA programs and include extensive data or theoretical analysis. Includes compilations of significant scientific and technical data and information deemed to be of continuing reference value. NASA counter-part of peer-reviewed formal professional papers, but has less stringent limitations on manuscript length and extent of graphic presentations.

- TECHNICAL MEMORANDUM. Scientific and technical findings that are preliminary or of specialized interest, e.g., "quick-release" reports, working papers, and bibliographies that contain minimal annotation. Does not contain extensive analysis.

- CONTRACTOR REPORT. Scientific and technical findings by NASA-sponsored contractors and grantees.

- CONFERENCE PUBLICATION. Collected papers from scientific and technical conferences, symposia, seminars, or other meetings sponsored or co-sponsored by NASA.

- SPECIAL PUBLICATION. Scientific, technical, or historical information from NASA programs, projects, and missions, often concerned with subjects having substantial public interest.

- TECHNICAL TRANSLATION. English-language translations of foreign scientific and technical material pertinent to NASA's mission.

For more information about the NASA STI program, see the following:

- Access the NASA STI program home page at http://www.sti.nasa.gov

- E-mail your question to help@sti.nasa.gov

- Fax your question to the NASA STI Information Desk at 757-864-6500

- Telephone the NASA STI Information Desk at 757-864-9658

- Write to:
  NASA STI Program
  Mail Stop 148
  NASA Langley Research Center
  Hampton, VA 23681-2199

NASA/TM—2016-219124

Multiscale Modeling of Carbon/Phenolic Composite Thermal Protection Materials: Atomistic to Effective Properties

Steven M. Arnold, Pappu L. Murthy, and Brett A. Bednarcyk
Glenn Research Center, Cleveland, Ohio

John W. Lawson
Ames Research Center, Moffett Field, California

Joshua D. Monk
Analytical Mechanics, Inc., Moffett Field, California

Charles W. Bauschlicher, Jr.
Ames Research Center, Moffett Field, California

National Aeronautics and
Space Administration

Glenn Research Center
Cleveland, Ohio 44135

July 2016

Trade names and trademarks are used in this report for identification only. Their usage does not constitute an official endorsement, either expressed or implied, by the National Aeronautics and Space Administration.

This work was sponsored by the Fundamental Aeronautics Program at the NASA Glenn Research Center.

Level of Review: This material has been technically reviewed by technical management.

Available from

NASA STI Program
Mail Stop 148
NASA Langley Research Center
Hampton, VA 23681-2199

National Technical Information Service
5285 Port Royal Road
Springfield, VA 22161
703-605-6000

This report is available in electronic form at http://www.sti.nasa.gov/ and http://ntrs.nasa.gov/

Multiscale Modeling of Carbon/Phenolic Composite Thermal Protection Materials: Atomistic to Effective Properties

Steven M. Arnold, Pappu L. Murthy, and Brett A. Bednarcyk
National Aeronautics and Space Administration
Glenn Research Center
Cleveland, Ohio 44135

John W. Lawson
National Aeronautics and Space Administration
Ames Research Center
Moffett Field, California 94035

Joshua D. Monk
Analytical Mechanics, Inc.
Moffett Field, California 94035

Charles W. Bauschlicher, Jr.
National Aeronautics and Space Administration
Ames Research Center
Moffett Field, California 94035

Abstract

Next generation ablative thermal protection systems are expected to consist of 3D woven composite architectures. It is well known that composites can be tailored to achieve desired mechanical and thermal properties in various directions and thus can be made fit-for-purpose if the proper combination of constituent materials and microstructures can be realized. In the present work, the first, multiscale, atomistically-informed, computational analysis of mechanical and thermal properties of a present day – Carbon/Phenolic composite Thermal Protection System (TPS) material is conducted. Model results are compared to measured in-plane and out-of-plane mechanical and thermal properties to validate the computational approach. Results indicate that given sufficient microstructural fidelity, along with lower-scale, constituent properties derived from molecular dynamics simulations, accurate composite level (effective) thermo-elastic properties can be obtained. This suggests that next generation TPS properties can be accurately estimated via atomistically informed multiscale analysis.

Introduction

Heat shields for space vehicles entering planetary atmospheres at hypersonic velocities experience some of the most severe operating conditions of any materials application. Thermal Protection System (TPS) materials, which are foundational to these heat shields, are typically ablative composites consisting of carbon fiber reinforcement with a phenolic resin matrix. Even with only two constituents, a considerable number of composite architectures are possible. In recent decades, several different ablative materials have been utilized for reentry TPS for NASA space missions. The phenolic impregnated carbon ablator (PICA) was developed in the early 1990s for mid-range heat flux environments and was used, for example, for the Curiosity rover Mars landing (Ref. 1). PICA is a low-density ablator consisting of a random, chopped fiber substrate with a high surface area phenolic resin. More demanding entry scenarios require higher density materials such as the heritage ablative composite Carbon/Phenolic which is made of a 2D carbon cloth with a fully dense phenolic resin (Ref. 2). Carbon/Phenolic was the heat shield material for the Galileo Jupiter mission, which is considered the most challenging entry environment experienced to date. It is also used in solid rocket engine applications.

Despite the success of PICA, Carbon/Phenolic, and other related materials for reentry TPS, the range of potential mission requirements are not fully covered by currently available materials. In response to this so-called “TPS gap”, a new class of materials based on woven 3D carbon composites has been investigated recently (Ref. 3). Woven materials considerably expand the design space of TPS materials by allowing for different weave architectures, fiber combinations, resin types and morphology. In addition to novel woven architectures, alternative resin systems have also been an active area of both computational and experimental investigation for next generation TPS. Navigation of this expanded material design space will benefit considerably from computational tools that can predict composite level properties based on composite architecture as well as constituent and interfacial properties.

The demonstration of just such an atomistically informed multiscale[1] analysis tool is the primary objective of this paper. Here, we perform the first, multiscale computational analysis of the mechanical and thermal properties of a TPS composite; wherein micromechanics and molecular dynamics are combined to demonstrate how ultimately design of new material systems can be achieved. In particular, we consider the important case of woven carbon cloth Carbon/Phenolic composites as a first step for consideration of the more general class of woven TPS materials. Micromechanical evaluations were accomplished using the MultiScale Generalize Method of Cells (MSGMC), see References 4 to 6, to transition the various levels of scales illustrated in Figure 1. Previous MSGMC work (Refs. 4 to 6), demonstrated the influence of scale-specific architectural features (e.g., tow fiber volume fraction, tow aspect ratio, tow void volume fraction, weave void distribution, void shape of woven composites) on woven composite response from a deterministic (Refs. 4 and 5) and stochastic (Ref. 6) viewpoint. Here the objective is to demonstrate how introducing “atomistically” informed constituent properties hierarchically and accurately accounting for microstructural features in a synergistic multiscale analysis framework, enables accurate prediction of woven TPS mechanical and thermal composite properties. Specifically, phenolic resin properties were obtained from molecular dynamics simulations whereas carbon fiber properties were drawn from the experimental literature. Computed thermal and mechanical composite level properties are compared to experimental data to validate this approach. In this study, as in our previous work, nesting/ply shifting of the woven composite layers was not considered.

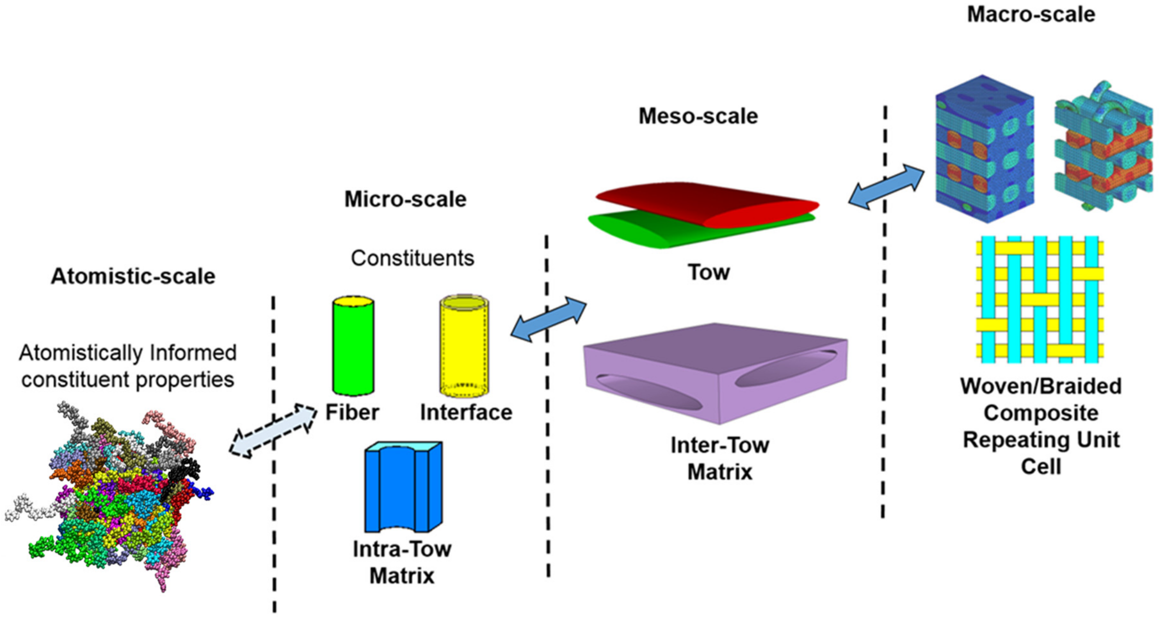

Figure 1.—Illustration of levels of scale included in modeling the woven TPS composite. The macro- meso- and micro-scales were considered in a synergistically coupled MSGMC analysis, while the atomistic-scale was included using an uncoupled hierarchical procedure.

---

[1] Here the term multiscale refers to an analysis in which at least three levels of scale are accounted for, wherein at least two homogenizations/localizations are required.

GMC Modeling Approach

The Generalized Method of Cells (GMC) micromechanics theory is an efficient, semi-analytical method that provides the homogenized, nonlinear constitutive response of a composite material. Its foundations for single scale analysis, along with validation of its results, are well-established in the literature (c.f. Ref. 7). The GMC method considers the composite microstructure, on a given length scale, to be periodic, with a repeating unit cell (RUC) as shown (at a given length scale) in Figure 2. The unit cell is discretized into N_α by N_β by N_γ subcells, each of which may contain a distinct material. However, as indicated in Figure 2, the unique feature of MSGMC is that the materials occupying the subcells on a given length scale, may themselves be heterogeneous composite materials, represented by a unique RUC. A given analysis may consist of an arbitrary number of explicit length scales, denoted by k (see Figure 2). The highest length scale considered is denoted as level 0, whereas, the current length scale under consideration is length scale i.

The GMC theory assumes a first-order displacement field in the subcells at a given scale, resulting in constant stresses and strains per subcell. Assuming infinitesimal strains, for the elastic case considered herein, the constitutive equation for the subcells at level i is given by,

$$\boldsymbol{\sigma}_i^{(\alpha_i\beta_i\gamma_i)} = \mathbf{C}_i^{(\alpha_i\beta_i\gamma_i)}\boldsymbol{\varepsilon}_i^{(\alpha_i\beta_i\gamma_i)} \tag{1}$$

where $\boldsymbol{\sigma}_i$ is the stress tensor, $\mathbf{C}_i$ is the stiffness tensor, and $\boldsymbol{\varepsilon}_i$ is the strain tensor. The superscript $(\alpha_i\,\beta_i\,\gamma_i)$ denotes the particular subcell at level i. Note that the method is not limited to the linear elastic case considered here, and previous work (Refs. 4 to 7) have included nonlinearity due to damage and inelasticity.

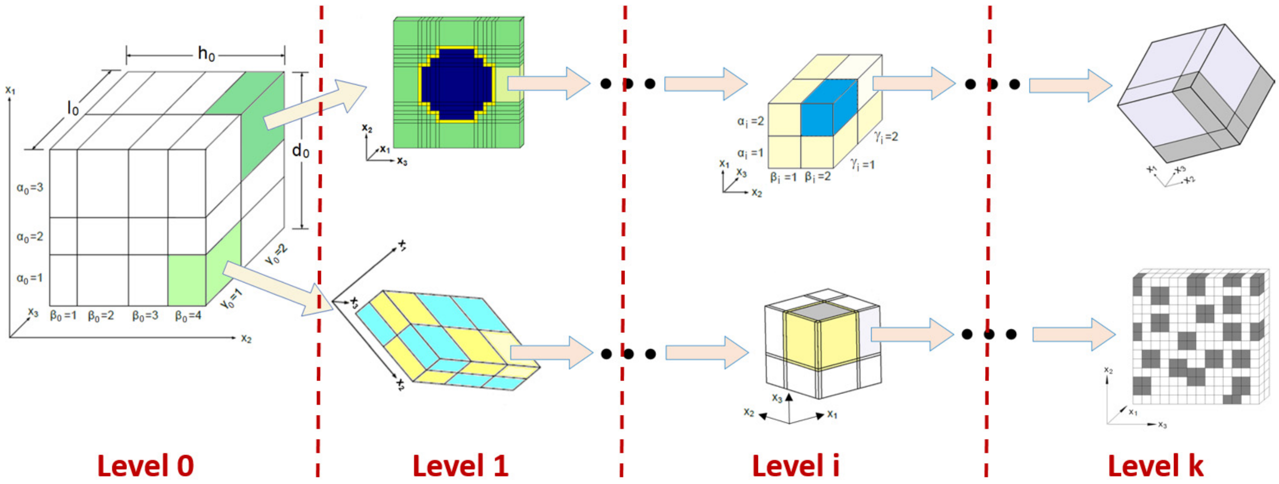

Figure 2.—MSGMC repeating unit cells (RUCs) and subcells across an arbitrary number of length scales.

Satisfaction of displacement and traction continuity between subcells in an average (integral) sense, and imposition of periodicity conditions along the repeating unit cell boundaries enable the establishment of a system of linear algebraic equations, which can be solved to determine the strain concentration tensor, $\mathbf{A}_i^{(\alpha_i\beta_i\gamma_i)}$. Details are given by Aboudi et al. (Ref. 7). At a given level of scale, *i*, this concentration tensor provide the local strain tensors in the subcells in terms of the RUC average strain tensor, $\bar{\boldsymbol{\varepsilon}}_i$,

$$\boldsymbol{\varepsilon}_i^{(\alpha_i\beta_i\gamma_i)} = \mathbf{A}_i^{(\alpha_i\beta_i\gamma_i)}\bar{\boldsymbol{\varepsilon}}_i \tag{2}$$

Note that, within a multiscale analysis, all terms in Equation (2) depend on the location of the level *i* RUC within all higher scale RUCs. That is, referring to Figure 2, the strain in a given subcell at level *k* depends on the path taken down the length scales from level 0.

Substituting Equation (2) into Equation (1),

$$\boldsymbol{\sigma}_i^{(\alpha_i\beta_i\gamma_i)} = \mathbf{C}_i^{(\alpha_i\beta_i\gamma_i)}\mathbf{A}_i^{(\alpha_i\beta_i\gamma_i)}\bar{\boldsymbol{\varepsilon}}_i \tag{3}$$

The RUC average stress tensor is given by,

$$\bar{\boldsymbol{\sigma}}_i = \frac{1}{d_i h_i l_i}\sum_{\alpha_i=1}^{N_{\alpha_i}}\sum_{\beta_i=1}^{N_{\beta_i}}\sum_{\gamma_i=1}^{N_{\gamma_i}} d_{\alpha_i} h_{\beta_i} l_{\gamma_i}\boldsymbol{\sigma}_i^{(\alpha_i\beta_i\gamma_i)} \tag{4}$$

where d_{α_i}, h_{β_i}, l_{γ_i} are the dimensions of subcell ($\alpha_i\,\beta_i\,\gamma_i$) and d_i, h_i, l_i are the RUC dimensions for level *i*. Equations (3) and (4) lead to,

$$\bar{\boldsymbol{\sigma}}_i = \frac{1}{d_i h_i l_i}\sum_{\alpha_i=1}^{N_{\alpha_i}}\sum_{\beta_i=1}^{N_{\beta_i}}\sum_{\gamma_i=1}^{N_{\gamma_i}} d_{\alpha_i} h_{\beta_i} l_{\gamma_i}\mathbf{C}_i^{(\alpha_i\beta_i\gamma_i)}\mathbf{A}_i^{(\alpha_i\beta_i\gamma_i)}\bar{\boldsymbol{\varepsilon}}_i \tag{5}$$

And recognizing that the effective elastic constitutive equation at level *i* is given by,

$$\bar{\boldsymbol{\sigma}}_i = \mathbf{C}_i^*\,\bar{\boldsymbol{\varepsilon}}_i \tag{6}$$

Equations (5) and (6) indicate that the effective stiffness tensor, $\mathbf{C}_i^*$, at level *i* is given by,

$$\mathbf{C}_i^* = \frac{1}{d_i h_i l_i}\sum_{\alpha_i=1}^{N_{\alpha_i}}\sum_{\beta_i=1}^{N_{\beta_i}}\sum_{\gamma_i=1}^{N_{\gamma_i}} d_{\alpha_i} h_{\beta_i} l_{\gamma_i}\mathbf{C}_i^{(\alpha_i\beta_i\gamma_i)}\mathbf{A}_i^{(\alpha_i\beta_i\gamma_i)} \tag{7}$$

In MSGMC, the scales are linked because the RUC average stress, strain, and stiffness tensors are equal to the local subcell stress, strain, and stiffness tensors of the applicable subcell from the next higher length scale (with appropriate transformation to account for the potential coordinate system change from scale to scale). That is,

$$\bar{\boldsymbol{\varepsilon}}_i = \mathbf{T}_2^i\,\boldsymbol{\varepsilon}_{i-1}^{(\alpha_{i-1}\beta_{i-1}\gamma_{i-1})},\ \bar{\boldsymbol{\sigma}}_i = \mathbf{T}_2^i\,\boldsymbol{\sigma}_{i-1}^{(\alpha_{i-1}\beta_{i-1}\gamma_{i-1})},\ \mathbf{C}_i^* = \mathbf{T}_4^i\,\mathbf{C}_{i-1}^{(\alpha_{i-1}\beta_{i-1}\gamma_{i-1})}, \tag{8}$$

where $\mathbf{T}_2^i$ and $\mathbf{T}_4^i$ are the appropriate second and fourth order coordinate transformation tensors, respectively. Hence, it is clear that, starting with the lowest scale (*k*) RUC (see Figure 2), whose subcells contain only monolithic materials, the effective stiffness tensor can be calculated using the standard GMC method. This stiffness tensor (after appropriate coordinate transformation) then represents the homogenized material in one of the subcells within an RUC at the next higher length scale. Given the transformed effective stiffness tensors of all subcells at this next higher length scale, the effective stiffness tensor of the RUC at this level can be determined. This stiffness tensor can then be transformed and passed along to the next higher length scale, and the process repeats until the highest length scale considered (0) is reached.

As an example, for an MSGMC analysis considering three length scales (0, 1, and 2), the overall effective stiffness tensor can be written using Equations (7) and (8) and as,

$$\mathbf{C}_0^* = \frac{1}{d_0 h_0 l_0} \sum_{\alpha_0 \beta_0 \gamma_0} d_{\alpha_0} h_{\beta_0} l_{\gamma_0} \left\{ \frac{\left(\mathbf{T}_4^1\right)^{-1}}{d_1 h_1 l_1} \sum_{\alpha_1 \beta_1 \gamma_1} d_{\alpha_1} h_{\beta_1} l_{\gamma_1} \left[\frac{\left(\mathbf{T}_4^2\right)^{-1}}{d_2 h_2 l_2} \sum_{\alpha_2 \beta_2 \gamma_2} d_{\alpha_2} h_{\beta_2} l_{\gamma_2} \mathbf{C}_2^{(\alpha_2 \beta_2 \gamma_2)} \mathbf{A}_2^{(\alpha_2 \beta_2 \gamma_2)} \right]^{(\alpha_1 \beta_1 \gamma_1)} \mathbf{A}_1^{(\alpha_1 \beta_1 \gamma_1)} \right\}^{(\alpha_0 \beta_0 \gamma_0)} \mathbf{A}_0^{(\alpha_0 \beta_0 \gamma_0)} \tag{9}$$

where a contracted notation has been used for the triple summation at each scale. Note that, in Equation (9), the superscript on the bracketed terms indicates that all variables within the brackets are a function of the subcell indices from the next higher length scale (including lower scale dimensions and subcell indices). The intent of this notation is to fully define the location of a subcell at a given scale as one progresses down the length scales. For example, using this notation, the effective stiffness tensor at level 2, from Equation (8), can be written as,

$$\left\{ \left[\mathbf{C}_2^* \right]^{(\alpha_1 \beta_1 \gamma_1)} \right\}^{(\alpha_0 \beta_0 \gamma_0)} = \left\{ \left[\mathbf{T}_4^2 \right]^{(\alpha_1 \beta_1 \gamma_1)} \right\}^{(\alpha_0 \beta_0 \gamma_0)} \left\{ \mathbf{C}_1^{(\alpha_1 \beta_1 \gamma_1)} \right\}^{(\alpha_0 \beta_0 \gamma_0)} \tag{10}$$

as there are distinct $\mathbf{C}_2^*$ values for every level 1 subcell, while there are distinct level 1 RUCs present within each level 0 subcell.

Converse to this multiscale homogenization procedure, MSGMC can perform multiscale localization of the stress and strain tensors. While not employed herein because only effective properties are presented for the TPS material considered, the multiscale localization is needed for inclusion of nonlinearity from damage and inelasticity (see Refs. 5 to 7). For the three length scale example, the local strain tensor in an arbitrary lowest scale (level 2) subcell can be written using Equations (2) and (8) as,

$$\left\{ \left[\boldsymbol{\varepsilon}_2^{(\alpha_2 \beta_2 \gamma_2)} \right]^{(\alpha_1 \beta_1 \gamma_1)} \right\}^{(\alpha_0 \beta_0 \gamma_0)} = \left\{ \left[\mathbf{A}_2^{(\alpha_2 \beta_2 \gamma_2)} \right]^{(\alpha_1 \beta_1 \gamma_1)} \right\}^{(\alpha_0 \beta_0 \gamma_0)} \left\{ \left[\mathbf{T}_2^2 \right]^{(\alpha_1 \beta_1 \gamma_1)} \right\}^{(\alpha_0 \beta_0 \gamma_0)} \left\{ \mathbf{A}_1^{(\alpha_1 \beta_1 \gamma_1)} \right\}^{(\alpha_0 \beta_0 \gamma_0)} \left\{ \mathbf{T}_2^1 \right\}^{(\alpha_0 \beta_0 \gamma_0)} \mathbf{A}_0^{(\alpha_0 \beta_0 \gamma_0)} \overline{\boldsymbol{\varepsilon}}_0 \tag{11}$$

Again, the superscript on the bracketed terms indicates that all variables within the brackets are a function of the subcell indices from the next higher length scale (including subcell indices). The stress tensor for any subcell at any length scale can be similarly determined through localization, or by simply using the strain tensor, along with the constitutive Equation (1), at the appropriate length scale. As will be discussed in the next section, because of its ability to handle multiple length scales in a single analysis, MSGMC is ideal for multiscale modeling of woven composite materials.

MSGMC Model: Weave Repeating Unit Cell

For the present study, a five harness satin (5HS) woven Carbon/Phenolic composite has been analyzed. In this idealization of the architecture, the repeating unit cell is assumed to be representative of the material contained within the coupon specimen used to measure the composite properties. A schematic of the 5HS fabric weave pattern, with its repeating unit cell (RUC) outlined in red, is shown in Figure 3. To create an RUC suitable for analysis, the weave is discretized into several subcells at this scale. There are two types of materials comprising all subcells: fiber tows and interweave matrix. The full three-dimensional discretization for a 5 HS composite is shown in Figure 4, along with the associated lower scale RUCs representing the multiscale analyses of the interweave inclusions, tows and intra-tow inclusions. In Figure 4, fiber tows are indicated through the lined subcells. The lines indicate the fiber orientation within the tows. The blank (white region) subcells represent the interweave matrix. Consequently, the 5HS macroscale RUC is subdivided into 11×11×4 subcells, each with dimensions given by

$$\begin{aligned} D &= \{t/4,\, t/4,\, t/4,\, t/4\} \\ H &= \{\delta/2, w, \delta, w, \delta, w, \delta, w, \delta, w, \delta/2\} \\ L &= \{\delta/2, w, \delta, w, \delta, w, \delta, w, \delta, w, \delta/2\} \end{aligned} \tag{12}$$

where the dimensions t, δ, and w are indicated in Figure 4. Within the context of GMC, the most important parameters are those related to volume fraction, v_f, specifically the overall V_f and the local tow V_{ftow}. The angle of undulation, herein taken as 20°, is the next most important parameter because it is responsible for the undulation and out of plane properties. The last parameter, tow spacing, is backed out to ensure geometric consistency by the following relationship $V_f = wV_{f_{\text{tow}}}/(w+\delta)$. In this equation w is the tow width and δ is the spacing with the proper overall V_f (herein held fixed at 0.38).

Herein constituent (fiber, resin, and carbon filler) volume fractions were determined from optical inspection (microscopy) of actual 5HS Carbon/Phenolic composites. Figure 5 illustrates the identified constituents (green). Note the corresponding volume fractions are 38, 48.5 and 13.5 percent, respectively. The carbon filler material, present within the phenolic matrix, was accounted for at a smaller length scale by analyzing a separate RUC and homogenizing those properties. This allows for a more efficient representation of inclusion shape and distribution than explicitly modeling inclusions at this higher length scale.

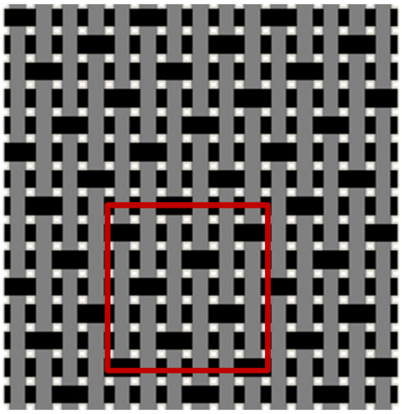

Figure 3.—Five harness satin repeating unit cell.

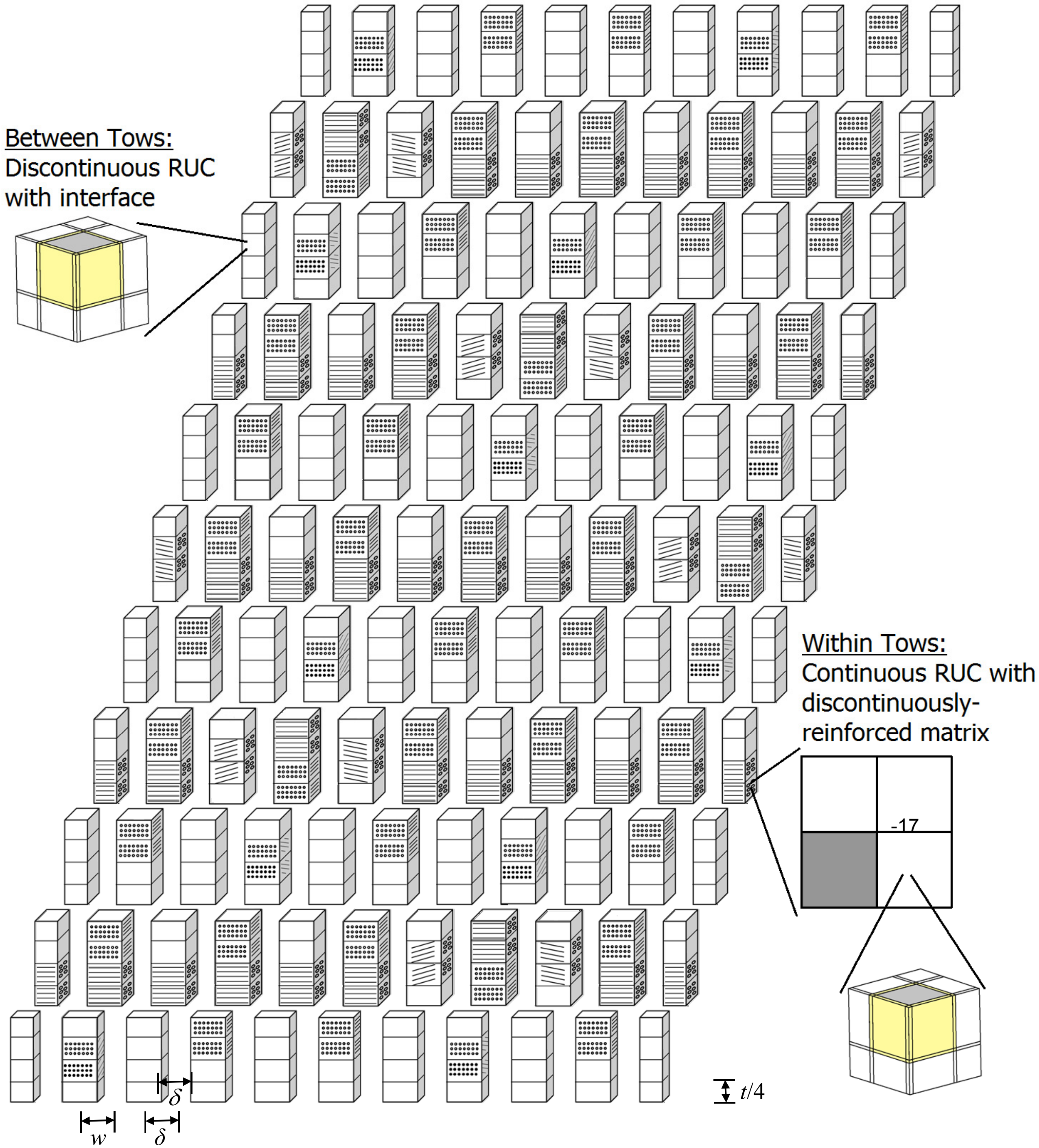

Figure 4.—Discretized 5HS satin woven composite RUC (not to scale), showing also the RUCs (not to scale) used to model the tow, as well as the discontinuously-reinforced inter-tow and intra-tow matrix.

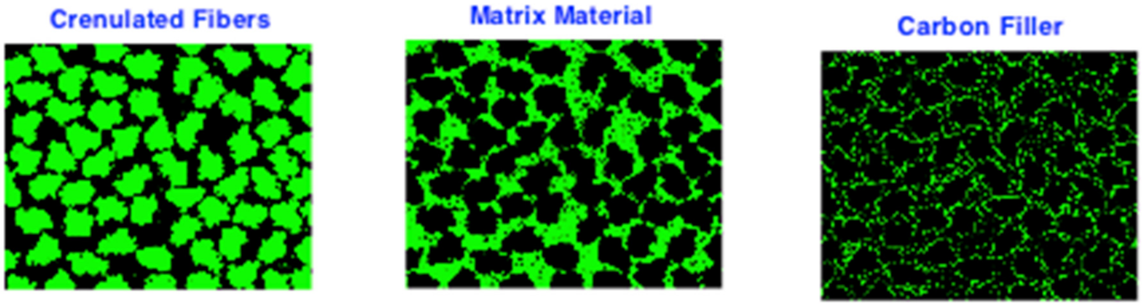

Figure 5.—Image analysis reveals constituents and associated volume fractions.

Constituent Properties

Molecular Dynamics (MD) Simulations

Phenolic resins have been a fundamental constituent of ablative materials for many decades due to their high char yield and good strength. The chemical structure of phenolic consists of phenol C_6H_5OH functional units connected by methylene $–CH_2$- linkers as shown in Figure 6. Uncured phenolic consists of low molecular weight oligomers, which form rigid, three-dimensional, thermoset networks upon crosslinking during cure. Crosslinking is accomplished by adding additional linkers between phenol rings. Typically, phenol can accommodate linkers at the two ortho sites (2,6) as well as at the para position (4) on the aromatic ring. Thus, phenolic rings can accommodate 1, 2 or 3 linkers. During cure, the density of linkers increases such that most phenol rings are linked by three cross-links, resulting in the formation of a full 3D polymer network.

To determine the mechanical and thermal elastic properties of the phenolic resin constituent (which constitute the input to the microscale analysis described previously, see Figure 1) molecular dynamics (MD) simulations of these systems were performed. MD simulations were performed with the Large-scale Atomic Molecular Massive Parallel Simulator (LAMMPS) software package (Ref. 12). The all-atom Optimized Potential for Liquid Systems (OPLS) force field parameters defined by Jorgensen (Ref. 13) were used.

To construct atomic models, we followed the algorithm described in previous work (Ref. 14). Briefly, systems of 50 independent linear chains with degree of polymerization equal to 9 were mixed and well-equilibrated. Chains in both the ortho-ortho and ortho-para configurations were considered. After equilibration of the independent chain system, cross-links were systematically introduced. We used a dynamic algorithm, where after reactive sites (ortho and para sites) were identified, the system was allowed to evolve dynamically. If the reactive sites approached each other within a pre-defined radius, a methylene linker was inserted between the two sites. After insertion, a combination of energy minimization and dynamics was used to relax the newly cross-linked structure and to relieve any stress. Heating/cooling cycles between 800 and 300 K were then performed to relax the full network. This process was iterated until a maximum crosslinking fraction, DOC, of approximately 85 percent was achieved. The crosslinking fraction was defined as the fraction of phenol rings that have three linkers attached. Higher crosslinking fractions (>85 percent) are difficult to achieve for these systems due to steric effects. After all the crosslinks have been added for a specified D, a final heating/cooling cycle was performed to arrive at the final structures. Using this algorithm, we derived a series of atomistic models as a function of cross-linking. A detailed study of the crosslinking algorithm and optimal parameters was reported in a recent publication (Ref. 14). Example of atomistic structures for uncrosslinked, percolating/gels and fully crosslinked structures are shown in Figure 7.

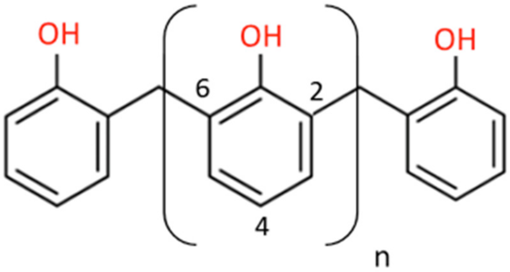

Figure 6.—Phenolic chain in an ortho-ortho configuration. Aromatic and methylene hydrogens are not shown for clarity.

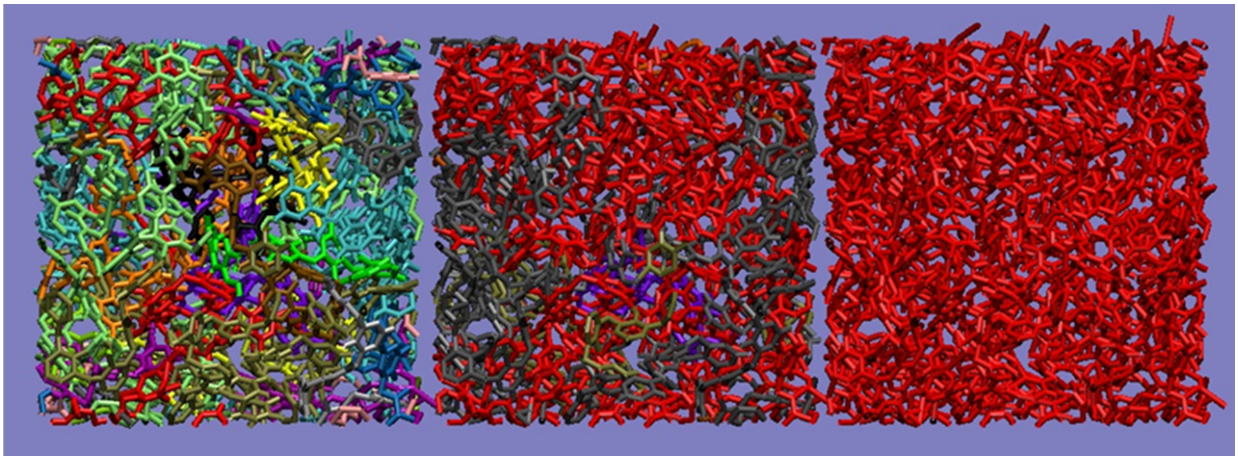

Figure 7.—Three phenolic structures at various degrees of cross-linking: (left) DOC = 0 percent, (middle) DOC = 24 percent and (right) DOC = 80 percent. Colors identify unique clusters within the system.

Once fully relaxed atomistic models were obtained, properties of the ideal volume of material could be evaluated. In recent work, we derived the complete set of properties including structural characterization, glass transition temperatures, elastic modulus, thermal conductivity, thermal expansion coefficients, etc. all as a function of temperature and crosslinking (Ref. 15). For the purposes of the present investigation, focus was given to the variation of the room temperature moduli and thermal conductivity as a function of cross-linking. Elastic moduli for the atomistic models were derived from stress strain curves obtained from virtual tensile, compression and shear deformation simulations. Continuous deformations were performed at different temperatures and the slope of the stress-strain curve was fit to obtain the Young’s modulus and the shear modulus. Topologically distinct phenolic networks were characterized in each coordinate direction and average values were obtained. Error bars were derived from a self-consistent Hill-Walpole method. Thermal conductivities were computed from equilibrium molecular simulations using the Green-Kubo approach. This method gives the lattice thermal conductivity as the time integral of the heat current autocorrelation function. Twenty nanosecond simulations averaged over topologically distinct configurations were performed for each degree of cross-linking.

Resin/Fibers

As already discussed, the basic constituents of TPS materials such as Carbon/Phenolic are the carbon fibers and the phenolic resin. Constituent level properties were used as input for the multiscale micromechanics computations. Carbon fibers derived from rayon precursors are typically used in TPS materials because of their low thermal conductivity and good mechanical properties. Fiber properties were not modeled explicitly (via MD) in this work since next generation TPS are expected to continue to

TABLE 1.—ROOM-TEMPERATURE CONSTITUENT PROPERTIES

Constituent	Property	Units	MD value	Experimental value	Used in MSGMC simulation
Resin	Young’s Modulus	GPa	4.13–5.5 [14–15]	3.5–5.79 [19,20,21,22]	4.13
	Poisson’s Ratio		0.34–0.37 [14–15]	0.36–0.37 [20,21	0.357
	Thermal Conductivity	W/m-K	0.30–0.34 [14–15]	0.25–0.32 [14,17,18]	0.295
Enka filament	Young’s Modulus	GPa		41.37 [26–28]	41.37
	Poisson’s Ratio			0.25 [23]	0.25
	Thermal Conductivity	W/m-K		3.7–4.1 [25–28]	3.9
Carbon filler	Young’s Modulus	GPa			311
	Poisson’s Ratio				0.17
	Thermal Conductivity	W/m-K			23.8
Interface	Young’s Modulus	GPa			1
	Poisson’s Ratio				0.3575
	Thermal Conductivity	W/m-K			0.0714

rely on rayon based carbon fibers (e.g., Enka filaments) and therefore, do not constitute a significant design variable at this time. Rather, improvements of TPS materials have focused on novel microstructures such as type of weave and alternative resins. Consequently, fiber properties were obtained from the literature and are reproduced in Table 1. Rayon fibers are known to have lower thermal conductivity than PAN or pitch-based fibers, which is a vital property in TPS materials. This is attributed to the disordered nature of the carbon crystallites that result from rayon fiber processing. However, due to the disordered arrangement within rayon fibers, their mechanical properties are significantly reduced compared to carbon fibers with more ordered graphitic atomic structures.

Elastic moduli and thermal conductivity for the phenolic constituent were obtained from atomistic simulations as a function of cross-linking, as described in the previous section. For example, data in Figure 8 shows higher cross-linked models result in higher elastic moduli, reflecting the higher rigidity of the 3D thermoset networks. Moduli obtained from simulations agree very well with experimental data performed on pure phenolic systems. Similarly, predicted thermal conductivity (as seen in Figure 8) shows an increasing trend as a function of cross-linking. This trend reflects the increase in thermal conduction pathways that become available as the cross-linking density increases. As with the moduli, thermal conductivity simulation results agree very well with experimental data - especially for high degrees of crosslinking.

In general, MD simulation results are expected to be upper bounds on the results for real systems. The simulations describe fully dense, defect free systems, whereas real systems will have non-trivial porosity, trapped condensation reaction products, mesoscale heterogeneity, etc. that will reduce these values. Structural characterization data on phenolic material suggests that fully cured phenolic is expected to be cross-linked on the order of ~80 percent. Therefore, phenolic simulation data for a range between 70 and 90 percent crosslinking is reported in Table 1. Values on the lower end of this range were used as input to the multiscale micromechanics computations since MD data are expected to be slight upper bounds. This choice is also consistent with experimental values, which are also reported in Table 1. As can be seen, agreement between the MD simulations and experiments is again very good. Therefore, we believe that the MD simulation results have sufficient experimental validation at the constituent level to give us significant confidence in their accuracy. Utilization of these “atomistically” informed constituent level thermoelastic properties thereby constitutes the handshake between MD simulations and micromechanical simulations of the actual woven TPS composite response (see Figure 8). Next, the Results Section will assess full multiscale predictions, wherein these MD properties were used as input at the lowest, continuum length scale.

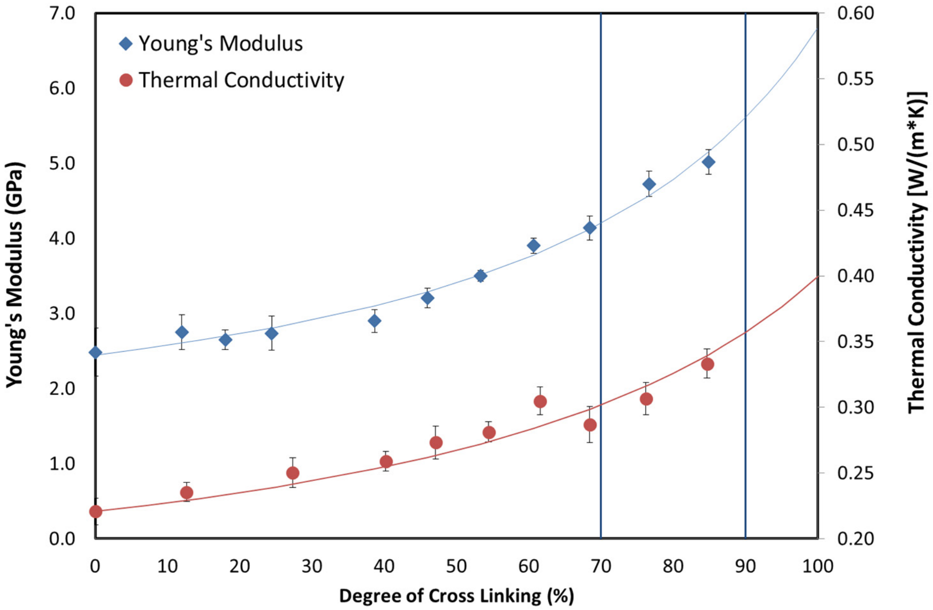

Figure 8.—Room temperature elastic modulus and thermal conductivity of phenolic resin constituent as a function of cross-linking as obtained from molecular dynamic simulations. Vertical lines indicate the lower and upper bounds defined in Table 1.

Results: Composite Properties

Elastic Properties: Pure Phenolic Resin Matrix

The 5HS Carbon/Phenolic composite was modeled using the MSGMC approach described previously. The global scale RUC is shown in Figure 4, with 11×11 in-plane subcells, and 4 subcells through the thickness. A tow width of $w = 220$ was employed, with a dimension between tows of $\delta = 104.2$ (units arbitrary) both dimensions obtained from a micrograph. Combined with a fiber volume fraction within the tows of 0.56, this gives an overall composite fiber volume fraction of 0.38, which matches the average measured value for the Carbon/Phenolic composite. The woven composite thickness is arbitrary as periodicity is assumed in this direction (as well as in the in-plane directions). Note also that, in the tow cross-over regions, a fiber angle of 20° was used.

As indicated in Figure 4, the composite tows were modeled using a simple 2×2 RUC representing the Enka carbon filament surrounded by the matrix material. For material properties, the room-temperature Enka filament properties (assumed to be isotropic) from Table 1 were used, whereas, for the resin, lower and upper bound values of the Young's modulus were used. These values were chosen as 4.13 and 5.5 GPa, respectively, to correspond to degrees of cross linking of 70 and 90 percent (see Figure 8). A fixed Poisson's ratio of 0.3575 was used for the isotropic resin. As a first step, the carbon filler material present within the phenolic resin (and shown in Figure 5) was not modeled. Rather, the matrix was simulated as neat phenolic resin – with MD properties and alternatively with deduced in-situ properties. As will be discussed below, parametric studies were performed to determine the best way to represent the resin, filler, and interface.

The in-plane and out-of-plane room-temperature Young's moduli predicted by the MSGMC analysis for the 5HS composite are compared with experimental values in Figure 9. Using the lower bound MD resin stiffness (4.13 GPa), the effective in-plane and out-of-plane composite moduli are under predicted by 22 and 27 percent, respectively. Using the upper bound MD value of 5.5 GPa, the moduli are still under predicted, but now by only 12 and 10 percent, respectively. Given that the upper bound (associated with 90 percent cross-linkage) exceeds the typical cross-linkage of 85 percent achievable in practice and that this bound is based on an ideal material, it is evident that utilization of the MD resin Young's modulus and literature

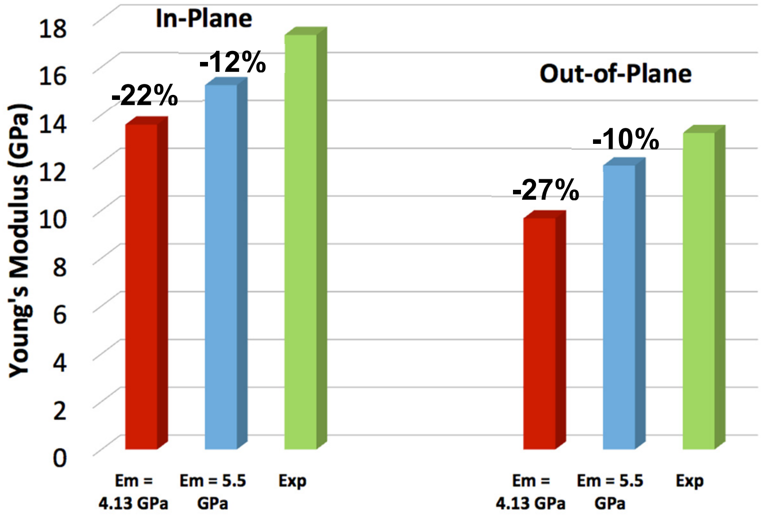

Figure 9.—Predicted Moduli at room temperature.

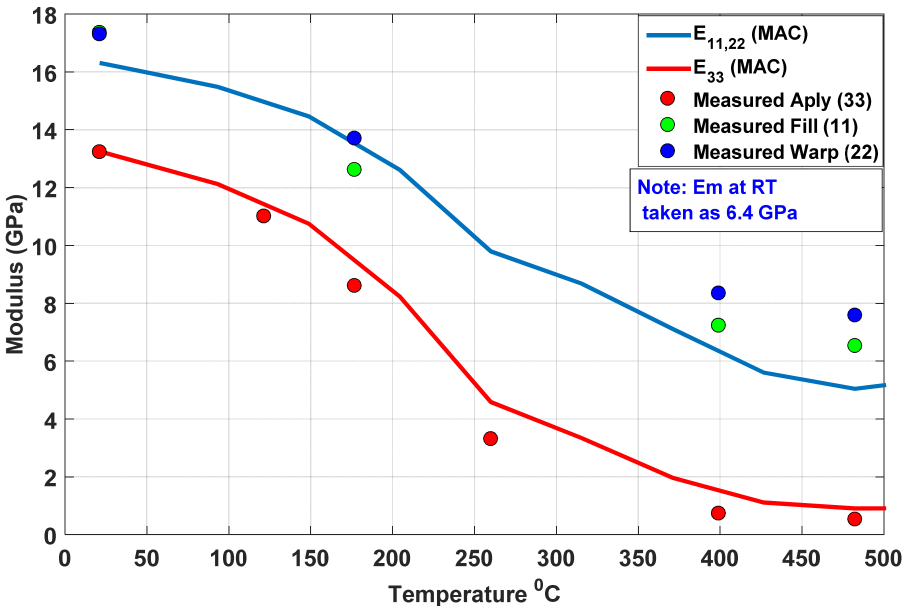

Figure 10.—Correlated in plane (11, 22) and out of plane (33) modulus as a function of temperature.

Enka fiber properties in conjunction with the employed MSGMC model does not capture accurately the associated experimentally measured Young's moduli of the composite. Clearly, when using MD resin properties neglecting the carbon filler within the resin is unacceptable. Note that the out-of-plane Young's modulus is known to be more directly dependent on the resin Young's modulus compared to the in-plane Young's modulus because of the predominantly in-plane orientation of the filaments. This is evident in the results of Figure 9, where the out-of-plane Young's modulus shows greater variation based on the variation in resin Young's modulus.

Alternatively, considering the resin stiffness to be an adjustable "model parameter", MSGMC can be used directly to reverse engineer an *in-situ* value for the phenolic Young's modulus so as to match the out-of-plane 5HS composite room-temperature Young's modulus. This value is 6.4 GPa, which is 16 percent higher than the upper bound predicted by MD. Figure 10 shows temperature-dependent experimental Young's modulus data for the composite. For use in the MSGMC model, temperature-dependent resin Young's modulus data were approximated by simply determining the ratio of the out-of-plane composite Young's modulus at each temperature to the room temperature value. These same ratios were then applied to obtain the in-situ resin Young's modulus for each temperature, while the Enka carbon fiber properties, as well as the resin Poisson's ratio, were held constant with temperature. The out-of-plane composite Young's moduli were used for this purpose since its magnitude is more dependent on that of the resin Young's modulus than is the in-plane moduli, due to the presence of continuous in-plane fibers. Indeed, it is clear from the experimental data in Figure 10 that the out-of-plane modulus of the composite exhibits a greater degree of temperature-dependence, which is consistent with the chosen approach to place all temperature-dependence in the resin Young's modulus. As shown in Figure 10, this approach enables reasonably good *correlation* between the MSGMC model results and the temperature-dependent experimental data, not only for the composite out-of-plane Young's modulus, but also for the in-plane Young's modulus.

Elastic Properties: Discontinuously Reinforced Phenolic Resin Matrix

An obvious source for the discrepancy between the room-temperature resin Young's modulus reversed engineered (6.4 GPa) to match the experimental data versus the upper bound, 90 percent cross-linked, MD prediction of the phenolic resin is the presence of the carbon filler within the phenolic resin itself (see Figure 5). This carbon filler (which discontinuously reinforces the phenolic resin) occupies 13.5 percent of the composite (21.8 percent of the matrix material) was not (nor could it be) included in the MD calculations. Consequently, to determine the effect of this carbon filler on the composite properties, the matrix (consisting of phenolic resin and the carbon filler as an inclusion) was modeled using a 3D GMC RUC, as shown in Figure 11.

A sensitivity analysis was performed to determine the impact of the various microstructural and material parameters (e.g., inclusion volume fraction, matrix stiffness, inclusion stiffness, and aspect ratio of the inclusion) on the effective properties of the discontinuously reinforced phenolic matrix. 1000 Monte Carlo simulations were performed assuming matrix and filler property values given in Table 2, a range of filler volume fraction (V.R.) between 10 and 15 percent and an inclusion aspect ratio range of 1 to 4. Note that, for parameters that were varied, a random value was chosen between the given ranges (i.e., uniform distribution) for each Monte Carlo instance.

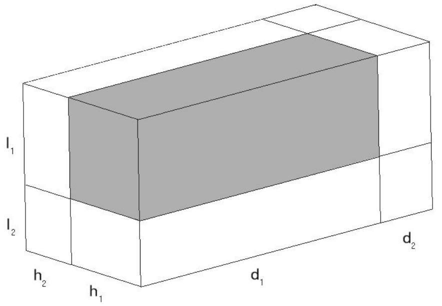

Figure 11.—Triply periodic RUC: Arch ID = 1, Aspect Ratio = d_1/h_1.

TABLE 2.—CONSTITUENT PROPERTIES

Constituent	Property	Units	Value
Resin	Young's Modulus	GPa	2.0–5.5
	Poisson's Ratio		0.357
Carbon filler	Young's Modulus	GPa	300–900
	Poisson's Ratio		0.17

The results of the Monte Carlo study are shown in Figure 12, wherein the calculated effective matrix Young’s modulus is plotted versus each of the four varied parameters, for each of the 1000 cases. Depending upon the particular parameter values for a given instance, the effective discontinuously reinforced matrix Young’s modulus ranges from approximately 2.5 to 8.8 GPa. It is thus clear that the target in-situ room-temperature matrix Young’s modulus of 6.4 GPa is achievable within the assumed parametric bounds. In addition, as parametric plots such as these appear more linear, like the plot associated with the resin modulus, stronger correlation is indicated. The calculated correlation coefficient from the Monte Carlo study for each parameter is plotted in Figure 13. Obviously, the matrix Young’s modulus has the dominant effect (greatest correlation coefficient) on the effective (discontinuously-reinforced matrix) Young’s modulus, with the remaining parameters having a much smaller influence (in decreasing order: aspect ratio, filler volume fraction, and filler Young’s modulus).

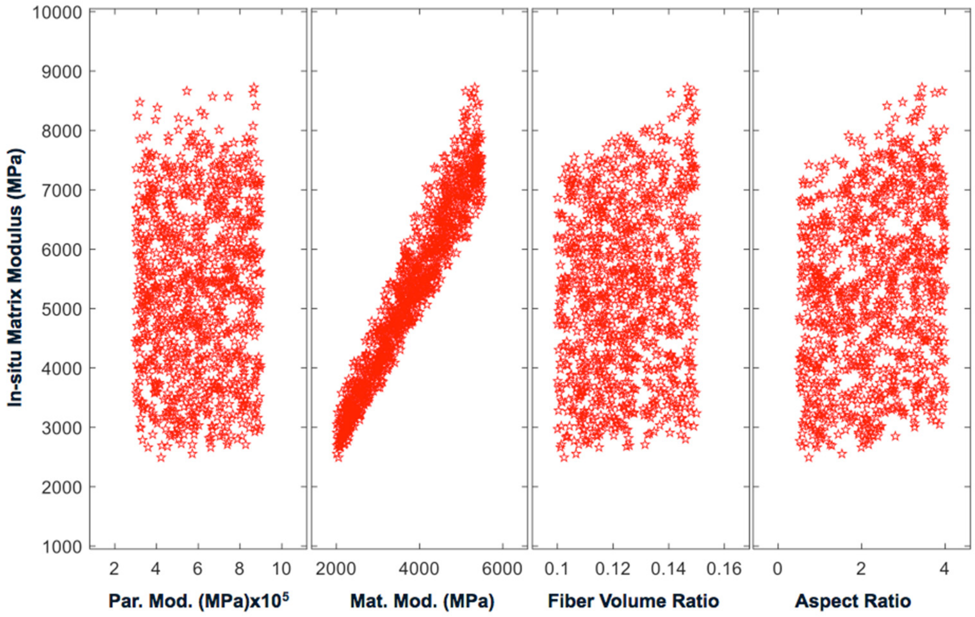

Figure 12.—Effective matrix modulus as a function of filler stiffness, matrix stiffness, filler volume fraction, and aspect ratio.

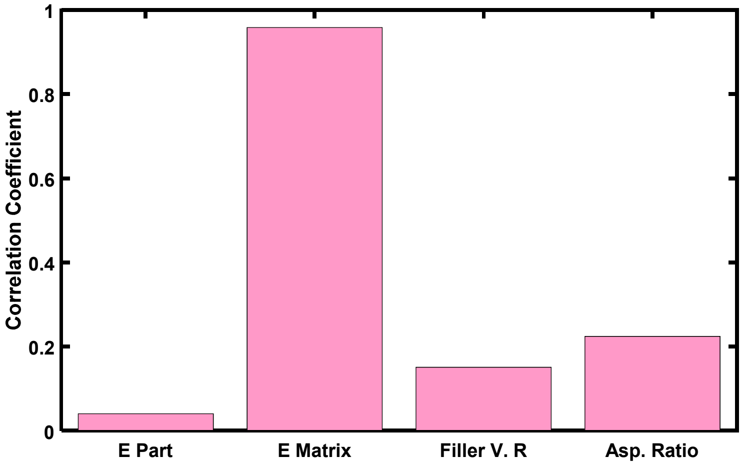

Figure 13.—Correlation coefficient for the material and geometric parameters studied.

In addition to the parameters examined above, the behavior of the interface between the carbon filler particles and the phenolic resin can influence the effective properties of the matrix. The impact of a compliant interface on the effective matrix properties was examined by explicitly including an interface phase/region, between the carbon filler and the phenolic resin, as shown in the lower scale GMC RUC in Figure 4 (with filler particle inclusion aspect ratio fixed at 1). The interface material's Young's modulus was varied from 0.1 GPa to either the upper (5.5 GPa) or lower (4.13 GPa) bound of the phenolic resin Young's modulus. The Poisson's ratio was kept the same as the phenolic resin as 0.3575. Two assumed interface volume fractions (I_{vr}), 1 and 5 percent. In all cases, the filler properties given in Table 1 were used, assuming a volume fraction of 13.5 percent. The results are plotted in Figure 14.

For all four cases, the effective matrix Young's modulus first rises rapidly with increasing interface Young's modulus, but then tends to plateau as the interface Young's modulus approaches that of the matrix, i.e., a strong bond. For the case of a thin interface (I_{vr} = 1 percent) this plateau initiates at approximately 1 GPa (approximately one-quarter of the phenolic resin lower bound). For the thicker interface this plateau is not reached until the interface modulus is equal to that of the resin matrix. Focusing on the target effective matrix Young's modulus of 6.4 GPa, it is clear from Figure 14 that assuming the lower bound for the phenolic resin Young's modulus in conjunction with a thin interface with 1 GPa Young's modulus, the targeted in-situ modulus can be achieved. Conversely, assuming a thicker interface (I_{vr} = 5 percent) in conjunction with a phenolic resin Young's modulus close to the average of the bounds can also achieve the target. Finally, if the upper bound phenolic resin Young's modulus is chosen, a much lower interfacial stiffness could be assumed and still achieve the target effective Young's modulus. Based on these results, the former option, with a lower bound (4.13 GPa) for the phenolic resin Young's modulus and a thin interface with 1 GPa Young's modulus was selected for use in the full multiscale simulations described below. Thus, the interface Young's modulus was taken to be roughly 1/4 (i.e., 24.2 percent) of the phenolic resin.

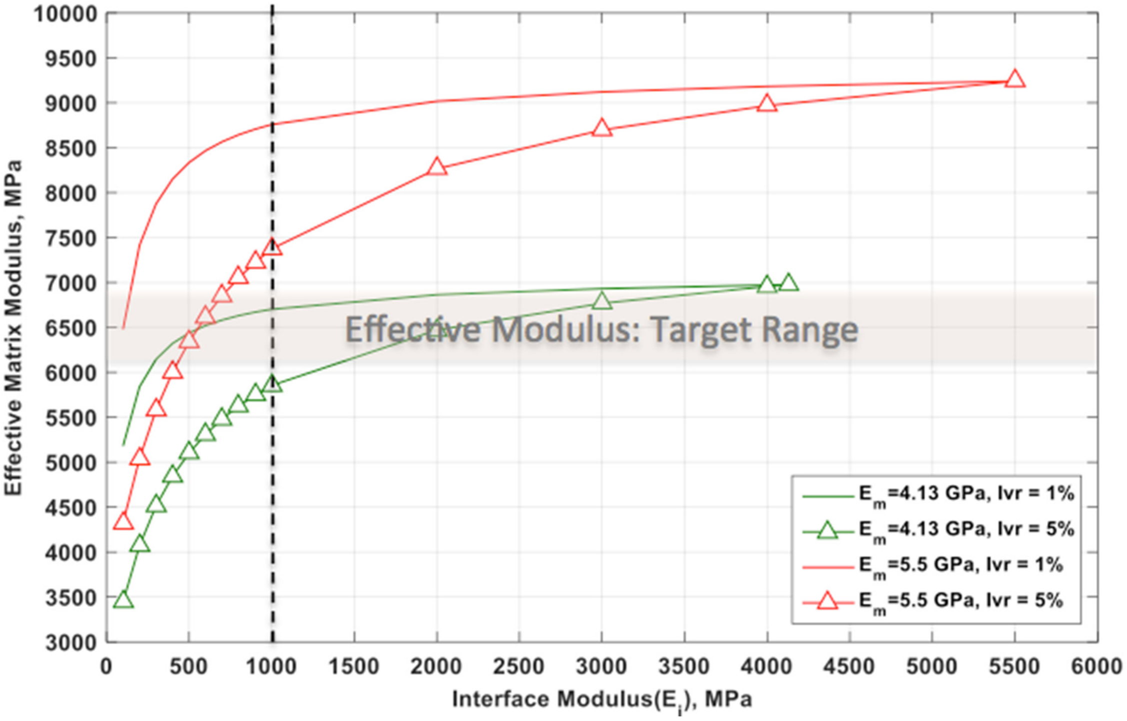

Figure 14.—Influence of imperfect bonding on effective matrix modulus.

Multiple four-level MSGMC analyses (see Figure 15) were performed to simulate the 2D woven Carbon Phenolic TPS composite properties as a function of temperature. This analysis was completed using the constituent properties in Table 1, the 5HS RUC shown in Figure 4, and the same temperature scaling for both resin and interface. Both the intra-tow and inter-tow matrix were considered to be phenolic resin with the Young's modulus set to the lower bound of 4.13 GPa. The matrix was discontinuously-reinforced by carbon filler particles with an aspect ratio of 1. The thin interfacial material, discussed above, was employed to represent compliant interfacial behavior between the resin and the carbon filler inclusions. Figure 15 shows a tree diagram of the multiscale simulations. The numbers on the tree diagram represent the number of subcells used for each branch on each scale. The total number of subcells employed on each scale is shown on the far right side of the figure. The total number of subcells across all scales is 103,341. While the four length scale shown in Figure 15 are fully coupled in the MSGMC analysis, it should be noted that the phenolic resin properties have been predicted from an uncoupled MD simulations. Therefore, the complete simulation of the 2D woven Carbon/Phenolic TPS composite actually represents five separate length scales, ranging from atoms (nanometers) to the woven RUC (millimeters); approximately six orders of magnitude. Furthermore the computational time required to perform an entire MSGMC simulation at a given temperature, using a single CPU, was approximately 300 sec.

Figure 16 shows the simulations of the in-plane and out-of-plane Young's moduli resulting from the full multiscale analysis as a function of temperature. All temperature-dependence in the predictions arises from the temperature-dependent properties employed for the phenolic resin (as discussed above) and the compliant filler/resin interface. The results indicate that the predicted effective composite Young's moduli, based on atomistically-informed properties and metallographically-informed microstructure, agree quite well with experimental measurements. Clearly, given sufficient microstructural information and MD provided constituent properties, the effective composite TPS properties (shown in Table 3 at room temperature) can be adequately predicted. Thus suggesting that next generation TPS properties can be accurately estimated via atomistically informed multiscale analysis.

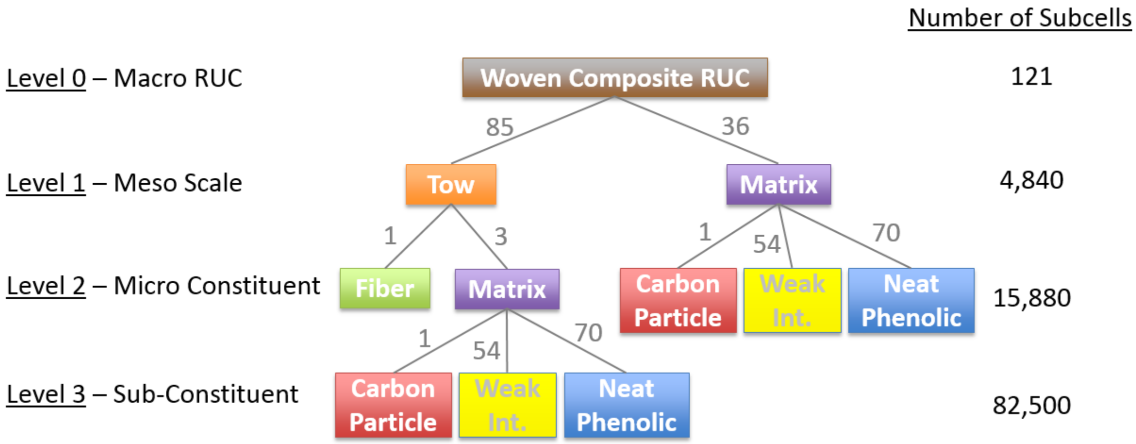

Figure 15.—Schematic tree diagram of the MSGMC multiscale simulation of the 5HS Carbon/Phenolic composite. The numbers indicate the number of subcells used in the simulation at each level of scale.

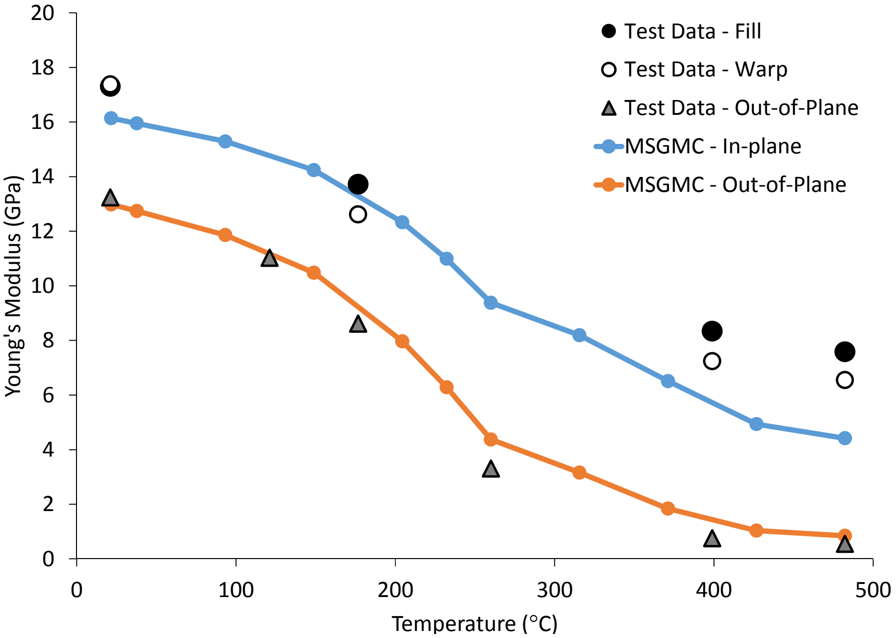

Figure 16.—5HS woven TPS composite response.

TABLE 3.—MSGMC PREDICTION OF RT
5HS CARBON/PHENOLIC COMPOSITE
WOVEN PROPERTIES

Property	Value
In-plane Young's modulus (GPa)	16.14
Out-of-plane Young's modulus (GPa)	12.98
In-plane shear modulus (GPa)	3.574
Out-of-plane shear modulus (GPa)	3.243
In-plane Poisson's ratio	0.228
Out-of-plane Poisson's ratio	0.240

Thermal Conductivity

In addition to predicting the mechanical properties of woven composites, MSGMC can predict effective thermal conductivities, given the thermal conductivities of the constituents (see Aboudi et al. (Ref. 7) for details). Figure 17 shows test data (Ref. 29) for the in-plane (warp and fill directions) and out-of-plane thermal conductivities of the 5HS Carbon/Phenolic composite as a function of temperature. Trend lines (based on quadratic best-fit) are also shown for the in-plane and out-of-plane data. The data show that, as expected, the in-plane thermal conductivity of the composite is higher due to the presence of continuous in-plane Enka carbon fibers (whose thermal conductivities are an order of magnitude higher than the phenolic matrix, see Table 1). Interestingly, however, the in-plane test data exhibit significantly more temperature-dependence than do the out-of-plane data. This is in contrast to the Young's modulus data (Figure 16), where the out-of-plane Young's modulus exhibited greater temperature-dependence. Because of this greater in-plane temperature-dependence for thermal conductivity, it is inconsistent to place all temperature-dependence on the phenolic resin conductivity, as was done in the case of Young's modulus. Rather, the out-of-plane composite thermal conductivity data were used to determine the phenolic resin thermal conductivity temperature-dependence, while the in-plane composite thermal conductivity data were used to determine the Enka fiber thermal conductivity temperature dependence. As such, the room-temperature Enka fiber and phenolic resin isotropic thermal conductivities (3.9 and 0.295 W/m-K, respectively) were scaled according to the trend lines plotted in Figure 17 to obtain their respective temperature-dependence.

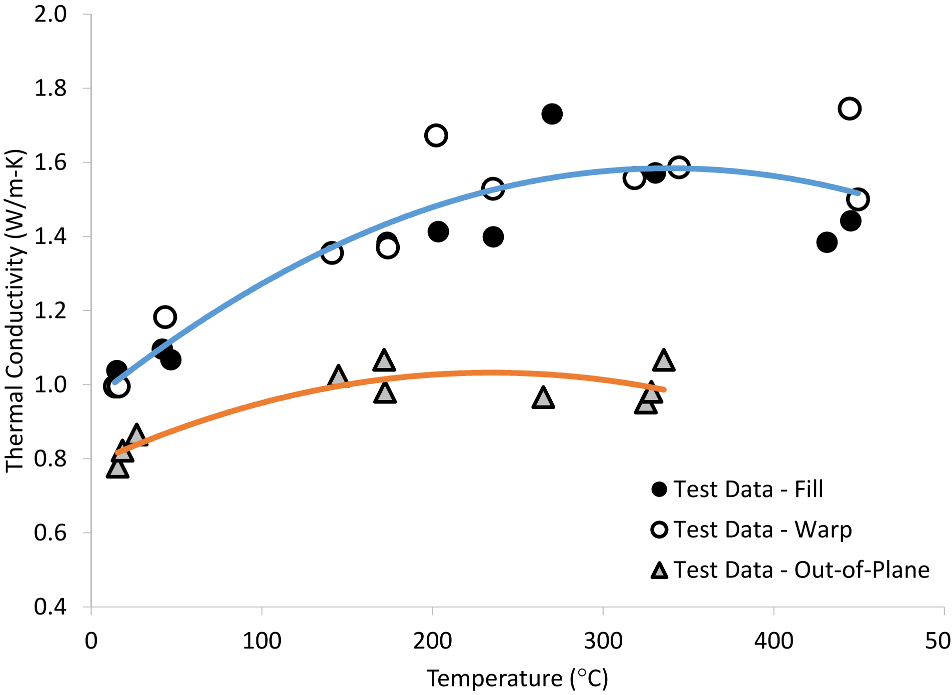

Figure 17.—Measured in-plane and out-of-plane thermal conductivities of the 5HS Carbon Phenolic composite as a function temperature, along with quadratic fit trend lines.

The carbon filler, as well as the interface between the carbon filler and the phenolic matrix, were once again accounted for in the identical manner as done in the mechanical analyses above (see Figure 4). The interface was taken to be identically effective in terms of thermal conductivity as it was mechanically. That is, the interface was assigned a thermal conductivity equal to 24.2 percent that of the phenolic resin at each temperature. The temperature dependence of all constituent properties was scaled according to the trend lines, except for the thermal conductivity of the carbon filler, which was taken to be independent of temperature.

The temperature-dependent effective thermal conductivities of the 5HS Carbon Phenolic composite were then calculated using MSGMC. Results are shown in Figure 18. For the out-of-plane thermal conductivity (solid line associated with triangular symbols) calculation (Figure 18), the MSGMC simulation is able to match the experimental data very well. The room-temperature simulation may be viewed as a prediction as the filler/resin interface thermal conductivity was not backed out from these test data (rather the mechanical interface characterization was employed). At other temperatures, however, these are not pure predictions as the resin temperature-dependence was gleaned from these data. The simulated in-plane thermal conductivity (solid line associated with circular symbols) is approximated 20 percent higher than the experimental data. The room-temperature simulation once again represents a prediction, whereas the other temperatures do not. The over prediction of the in-plane test data could indicate that the thermal conductivity of the Enka carbon fiber, which greatly influences the in-plane thermal conductivity, is too high. The effect of reducing the Enka fiber thermal conductivity by 20 percent (across all input temperatures) is illustrated by the dashed lines in Figure 18. Clearly, a good match with the experimental data is possible with a reduced Enka fiber thermal conductivity. This, however, also impacts the out-of-plane effective thermal conductivity of the composite, but to a lesser extent (approximately 6 percent), as also shown in Figure 18.

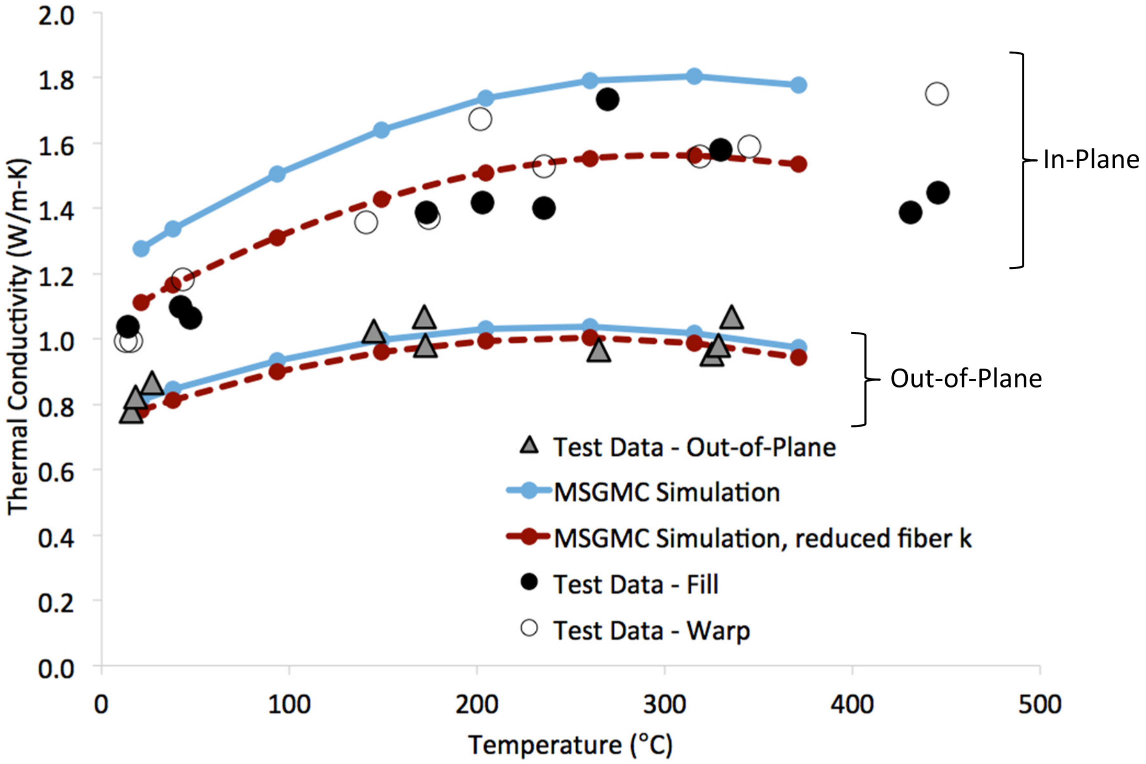

Figure 18.—MSGMC simulations of the temperature-dependent out-of-plane effective thermal conductivity of the 5HS Carbon Phenolic composite.

Conclusions

This paper presents a multiscale, atomistically-informed, computational analysis of mechanical and thermal properties of a present day – Carbon/Phenolic – composite Thermal Protection system (TPS) material. The recently implemented Multiscale Generalized Method of Cells (MSGMC) methodology was employed to incorporate "atomistically" informed constituent properties and detailed microstructural features in a coupled, synergistic multiscale analysis of a 5HS woven TPS composite material. Specifically, phenolic resin properties were obtained from molecular dynamics (MD) simulations whereas carbon fiber properties and carbon black filler material were drawn from the experimental literature. Such obtained constituent properties were then used as input for micromechanics computations. Results indicated that unless sufficient microstructural information was also included in the analysis MD properties could not be used directly, thus requiring the "adjustment" of in-situ model parameters like matrix modulus and conductivity. However, if one combined microstructural detail (i.e., continuously reinforced weave within a discontinuously-reinforced matrix) and lower-scale, molecular dynamically derived, constituent properties, accurate composite level (effective) in-plane and out-of-plane thermo-elastic properties can indeed be obtained. This suggests that next generation TPS properties can be accurately estimated at temperatures below charring via atomistically informed multiscale analysis.

References

1. Tran, H., Johnson, C., Rasky, D., Hui, F., Chen, Y.K. and Hsu, M.; “Phenolic Impregnated Carbon Ablator (PICA) for Discovery Class Missions,” AIAA Paper 96-1911, June 1996.
2. Metzger, J.W; “The behavior of ablating carbon phenolic,” AIAA Paper 72-363, April, 1972.
3. Arnold, J.O., Peterson, K.H., Yount, B.C., Schneider, N. and Chavez-Garcia, J.; AIAA Paper 2013-1370, March, 1013.
4. Liu, K. and Chattopadhyay, A. and Bednarcyk, B. and Arnold, S.M.; “Efficient Multiscale Modeling Framework for Triaxially Braided Composites Using Generalized Method of Cells,” Journal of Aerospace Engineering, April 2011.
5. Liu, K.C. and Arnold, S.M.; “Impact of Material and Architecture Model Parameters on the Failure of Woven CMCs Via the Multiscale Generalized Method of Cells,” NASA/TM—2011-217011.
6. Liu, K.C. and Arnold, S.M.; “Statistical Influence of Scale Specific Features on the Progressive Damage of Woven Ceramic Matrix Composites (CMCs),” Computers, Materials and Continua. Vol. 35, No. 1, 2013, pp. 35–65.
7. Aboudi, J., Arnold, S.M., and Bednarcyk, B.A.; (2013) Micromechanics of Composite Materials: A Generalized Multiscale Analysis Approach, Elsevier, Oxford, UK.
8. B.A. Bednarcyk and S.M. Arnold; “MAC/GMC 4.0 User’s Manual, Volume 2: Keywords Manual,” TM 2002-212077/Vol. 2, 2002.
9. Paley, M. and Aboudi, J.; “Micromechanical Analysis of Composites by the Generalized Method of Cells,” Mechanics of Materials 1992; 14: 127–139.
10. Aboudi, J.; “Micromechanical Analysis of Thermo-Inelastic Multiphase Short-Fiber Composites,” Composite Eng. 5, 839–850, 1995.
11. Bednarcyk, B. and Arnold, S.M.; “Micromechanics Based Modeling of Woven Polymer Matrix Composites,” AIAA Journal, Vol. 41, No. 9, pp. 1788–1796, 2003.
12. Plimpton, S.; “Fast Parallel Algorithms for Short-Range Molecular Dynamics,” J Comp Phys, Vol. 117, 1995, pp. 1–19.
13. Jorgensen, W.L., Maxwell, D.S., Tiradorives, J. “Development and testing of the OPLS all-atom force field on conformational energetics and properties of organic liquids,” J. Am. Chem. Soc., Vol. 118, 1996, pp. 11225–11236; Jorgensen, W.L. and Tirado-Rives, J. “The OPLS [optimized potentials for liquid simulations] potential functions for proteins, energy minimizations for crystals of cyclic peptides and crambin,” J. Am. Chem. Soc., Vol. 110, 1988, pp. 1657–1666; Cornell, W.D., Cieplak, P., Bayly, C.I., Gould, I.R., Merz, K.M., Ferguson, D.M., Spellmeyer, D.C., Fox, T., Caldwell, J.W., Kollman, P.A.,” A second generation force field for the simulation of proteins, nucleic acids, and organic molecules,” J. Am. Chem. Soc., Vol. 118, 1996, pp. 2309–2309.
14. Monk, J.D, Haskins, J.B., Bauschlicher, C.W. and Lawson, J.W.; “Molecular dynamics simulations of crosslinked phenolic resins: construction of atomic models,” Polymer 62 (2015), p. 39.
15. Monk, J.D., Bucholz, E.W., Boghozian, T., Deshpande, S., Schrieber, J., Bauschlicher, C.W. and Lawson, J.W.; “Computational and Experimental Study of Phenolic Resins: Thermal-Mechanical Properties and the Role of Hydrogen Bonding,” Macromolecule, (2015), submitted.
16. Warfield, R.W. and Kayser, E.G.; “Specific heat of phenolic polymer,” J. Macromol. Sci., Part B: Phys., Vol. B11, 1975, p. 325.
17. Mottram, J.T., Geary, B. and Taylor, R.; “Thermal expansion of phenolic resin and phenolic-fiber composites,” J. Mater. Sci., Vol. 27, 1992, p. 5015.
18. Patton, R.D., Pittman, C.U., Wang, L., Hill, J.R. and Day, A.; “Ablation, mechanical and thermal conductivity properties of vapor grown carbon fiber/phenolic matrix composites,” Compos. Part A: Appl. Sci. and Man., Vol. 33, 2002, p. 243.
19. Wang, Z.J., Kwon, D.J., Gu, G.Y., Lee, W.I., Park, J.K., DeVries, K.L., Par, J.M.; “Ablative and mechanical evaluation of CNT/phenolic composites by thermal and microstructural analyses,” Composites Part B: Eng, Vol. 60, 2014, p. 597.

20. Hartmann, B. “Ultrasonic properties of phenolic and poly (phenylquinoxaline) polymers,” J. of Appl. Poly. Sci, Vol. 19, 1975, p. 3241.
21. Harwood, C., Wostenholm, G.H. and Yates, B., “Thermodynamic properties of phenol–formaldehyde resin,” J. Polymer Sci., Vol. 16, 1978, p. 759.
22. Yeh, M.K., Tai, N.H. and Liu, J.H., “Mechanical behavior of phenolic-based composites reinforced with multi-walled carbon nanotubes,” Carbon, Vol. 44, 2006, p. 1.
23. Tellers, R., ATK Launch Systems Inc. Final Report TWR-76794.
24. Sauder, C. and Lamon, J.; “Prediction of elastic properties of carbon fibers and CVI matrices,” Carbon, Vol. 43, 2005, p. 2044.
25. Pradere, C., Batsale, J.C., Goyheche, J.M., Pailler, R., Dilhaire, S.; “Thermal properties of carbon fibers at very high temperature,” Carbon, Vol. 47, 2009, p. 737.
26. Rossi, R.C., and Wong, W.C.; “Availability of Aerospace Rayon for SRM Nozzle Insulators,” AIAA, 1996.
27. Pilato, L.A. and Michno, M.J. (1994); Advanced Composite Materials. Springer Science & Business Media.
28. Katzman, H.A., Adams, P.M, Le, T.D. and Hemminger. C.S. “Characterization of low thermal conductivity PAN-based carbon fibers,” Carbon, Vol. 32, 1994, p. 379.
29. Williams, A.R.; “Rayon Replacement Program Phase IV MX4926N MT Mechanical and Thermal Characterization,” SRI-ENG-07-34-9714.09, Final Report, Southern Research Institute, 2008.